Exploring the Relationship Between Multilayered Choroidal Neovascularization and Choriocapillaris Flow Deficits in AMD

Peter L. Nesper, Janice X. Ong, and Amani A. Fawzi

Department of Ophthalmology, Feinberg School of Medicine, Northwestern University, Chicago, Illinois, United States

Correspondence: Amani A. Fawzi, Department of Ophthalmology, Feinberg School of Medicine, Northwestern University, 645 N. Michigan Avenue, Suite 440, Chicago, IL 60611, USA; afawzimd@gmail.com.

Received: December 2, 2020
Accepted: February 5, 2021
Published: March 9, 2021

Citation: Nesper PL, Ong JX, Fawzi AA. Exploring the relationship between multilayered choroidal neovascularization and choriocapillaris flow deficits in AMD. *Invest Ophthalmol Vis Sci.* 2021;62(3):12. https://doi.org/10.1167/iovs.62.3.12

Purpose. We used optical coherence tomography angiography to test the hypothesis that more complex, multilayered choroidal neovascular (CNV) membranes in AMD are associated with worse flow deficits (FD) in the choriocapillaris.

Methods. Retrospective, cross-sectional study including 29 eyes of 29 subjects with neovascular AMD. En face choriocapillaris images were compensated for signal attenuation using the structural OCT slab and signal normalization based on a cohort of healthy subjects. We binarized the choriocapillaris using both local Phansalkar and global MinError(I) methods and quantified FD count, FD density, and mean FD size in the entire area outside the CNV, in the 200-µm annulus surrounding the CNV, and in the area outside the annulus. We used projection-resolved optical coherence tomography angiography to quantify CNV complexity, including highest CNV flow height, number of flow layers, and flow layer thickness. We explored the relationship between CNV complexity and choriocapillaris FD using Spearman correlations.

Results. The highest CNV flow signal significantly correlated with lower FD count ($P < 0.01$), higher FD density ($P < 0.05$), and higher mean FD size ($P < 0.05$) in the area outside the annulus and the entire area outside the CNV using both Phansalkar and MinError(I). Within the annulus, CNV complexity was not consistently correlated with choriocapillaris defects.

Conclusions. CNV vascular complexity is correlated with choriocapillaris FD outside the CNV area, providing evidence for the importance of choriocapillaris dysfunction in neovascular AMD, as well as the potential role of choroidal ischemia in the pathogenesis of complex CNV membranes.

Keywords: optical coherence tomography angiography, OCT, OCTA, macula, retina, choriocapillaris

AMD is a leading cause of blindness, affecting over 6 million people globally and more than 10% of people older than 80 years in the United States.[1,2] Neovascular AMD is an advanced stage of the disease characterized by the development of choroidal neovascular (CNV) membranes, where anomalous blood vessels break through Bruch's membrane and grow in the subretinal and sub-RPE cell spaces. Owing their immature cellular phenotype, CNV membranes leak intravascular components causing fluid accumulation, hemorrhage and vision loss.[3] Although the pathogenesis of CNV is not entirely understood, the process of angiogenesis is associated with the upregulation of VEGF, which is secreted by the RPE.[4,5] VEGF expression is increased in macular RPE cells in patients with AMD and its upregulation induces intrachoroidal neovascularization in experimental mouse models.[6,7] The role of this angiogenic growth factor is further highlighted by the therapeutic benefit of anti-VEGF in decreasing fluid exudation from CNV.[8,9]

Choriocapillaris dropout has been shown in the area surrounding the CNV membranes in AMD.[10–13] The loss of choriocapillaris around CNV has been observed even in areas of intact RPE in histopathologic studies, suggesting that choriocapillaris degeneration may be the initial structural insult in neovascular AMD.[10,14] Choriocapillaris dysregulation is also seen in early and intermediate AMD and is thought to contribute to RPE hypoxia,[14–16] which in turn could play an important role in promoting angiogenesis and continual vascular remodeling in eyes with AMD.[17,18] This aberrant angiogenic pathway in AMD may be similar of the pathogenesis of proliferative diabetic retinopathy (PDR) and retinopathy of prematurity, where retinal, instead of choroidal, vascular occlusion and the resultant ischemia act as the inciting stimulus for preretinal vascular proliferation.[19,20]

Optical coherence tomography angiography (OCTA) provides clinicians and researchers with high-resolution images of choroidal vasculature in vivo. Numerous studies have quantified CNV parameters in AMD, including a study from our group where we reported that more complex three-dimensional (3D) CNV parameters were associated with a higher frequency of anti-VEGF injections during individualized treatment protocols.[21] Based on the understanding

that VEGF is upregulated in cells exposed to ischemia,[22] we hypothesized that more flow deficits (FD) in the choriocapillaris on OCTA would be associated with greater CNV complexity in eyes with neovascular AMD. Using a semi-automated process to test this hypothesis, we compensated for drusen shadowing, retinal vessel projection, and signal strength variability before quantifying choriocapillaris FD using global and local binarization methods. In this quantitative study of the vasculature in CNV and the surrounding choriocapillaris, we discuss the potential interdependence of these two vascular compartments in neovascular AMD and provide a streamlined approach to choriocapillaris image processing based on the most recent studies.[23–25]

Methods

This retrospective, cross-sectional study included patients with CNV secondary to AMD in the Department of Ophthalmology at Northwestern University in Chicago, Illinois, between June 2015 and August 2019. The study was approved by the Institutional Review Board of Northwestern University and followed the tenets of the Declaration of Helsinki. The study was performed in accordance with the Health Insurance and Portability and Accountability Act regulations and written consent was obtained from all participants before participation.

Patient Criteria

Inclusion criteria were eyes with CNV secondary to AMD, based on clinical assessment by a retinal specialist (AAF). We included eyes with type 1 CNV (vascularized pigment epithelial detachment [PED]), type 2 CNV (subretinal), and type 4 CNV (polypoidal). Polypoidal choroidal vasculopathy (PCV) was diagnosed by the presence of a branching vascular network and polyps on indocyanine green angiography.[26,27] We included both treatment-naïve eyes and eyes previously treated with intravitreal anti-VEGF agents, including ranibizumab, bevacizumab, and/or aflibercept. Only eyes with a quality index score of Q6 or greater and without large motion artifacts were included in the study. For signal strength normalization, we also included a subset of 30 healthy eyes from 30 patients aged 20 to 30 years with a quality index score of Q9.

Exclusion criteria were eyes with other retinal disease, such as diabetic retinopathy, glaucoma, glaucoma suspects, type 3 (intraretinal) CNV, or occlusive diseases. Owing to a large number of OCTA studies showing early vascular changes in patients with diabetes mellitus (DM) without evidence of diabetic retinopathy, we also excluded eyes from any patient diagnosed with DM. We excluded eyes with high refractive error (fewer than −6 diopters), and those with cataracts graded above nuclear opalescence grade three or nuclear color grade three, to minimize artifacts that may compromise OCTA image quality.[28] If both eyes from an individual were eligible, the eye with better OCTA signal strength was included. Electronic medical records were reviewed to extract demographic and clinical information.

OCTA Imaging

We obtained 3 mm × 3 mm (304 pixels × 304 pixels) OCTA images using the RTVue-XR Avanti system (Optovue, Inc., Fremont, CA) with split-spectrum amplitude-decorrelation angiography software (version 2017.1.0.151).[29] This device uses a light source centered on 840 nm with a full-width at one-half maximum bandwidth of 45 nm and an A-scan rate of 70,000 scans per second. The RTVue OCTA system captures two consecutive B-scans (M-B frames) at each location on the retina, with each B-scan consisting of 304 A-scans. An orthogonal registration algorithm was used to decrease motion artifacts.[30] The split-spectrum amplitude-decorrelation angiography algorithm then quantifies the decorrelation of OCT reflectance between the two consecutive B-scans to provide angiographic information. Decorrelation represents the difference in OCT reflection between the two B-scans separated only by time, which is attributed to the movement of red cells.

Choriocapillaris Image Analysis

Choriocapillaris analysis was performed using the manufacturer's automated segmentation of 10 µm above to 30 µm below Bruch's membrane. We evaluated the automated segmentation, and any segmentation errors were manually corrected using the AngioVue Analytics software (2017.1.0.151). The OCTA and OCT of the choriocapillaris slab were exported into FIJI software,[31] a distribution of the program ImageJ.

A custom macro was implemented in FIJI to streamline the analysis of the choriocapillaris. The macro performed all the analysis steps, except for user-defined manual delineation of the CNV area. First, OCTA images were compensated for signal attenuation and shadowing artifacts using the OCT choriocapillaris slab.[32] Specifically, an inverse transformation and Gaussian blur of sigma 3.0 were applied to the OCT slab, after which the OCTA choriocapillaris slab was multiplied by the blurred, inverted OCT slab. The OCTA choriocapillaris slab was then normalized to a signal strength score of Q9 (Fig. 1).[33] To normalize the image, we first obtained the average pixel intensity of the choriocapillaris OCTA for a healthy population of 30 eyes from 30 subjects aged 20 to 30 years with a Q-score of Q9. For each eye in the AMD cohort, we calculated a fraction representing the average choriocapillaris pixel intensity from the Q9 group divided by the average choriocapillaris pixel intensity from the AMD eye. We then multiplied each pixel in the AMD choriocapillaris image by this fraction.

After drusen compensation and normalization, the choriocapillaris was binarized using two different thresholding approaches. We used these two methods to test the generalizability and internal validity of our study, because different binarization methods can produce varying results.[23] For local thresholding, we used the Phansalkar method with a pixel radius window of 2.0, consistent with the size of one to two intercapillary spaces in healthy eyes as suggested by recently published studies.[24,25,34] For global thresholding, we used the MinError(I) method, which assumes a normal distribution for both the object (FD) and the background (choriocapillaris).[35,36] We used this method because it produced binarized images with FD that showed qualitatively similar size and extent compared with the original choriocapillaris images. Before calculating FD parameters, we used the Max Entropy plugin to eliminate areas of potential shadowing or projection artifact from large superficial vessels.[37]

Using the polygon selection tool in FIJI, the CNV area was manually outlined and input into the macro for further calculations. We then enlarged the CNV area by 200 µm to yield an annulus or ring around the CNV. The FD measures

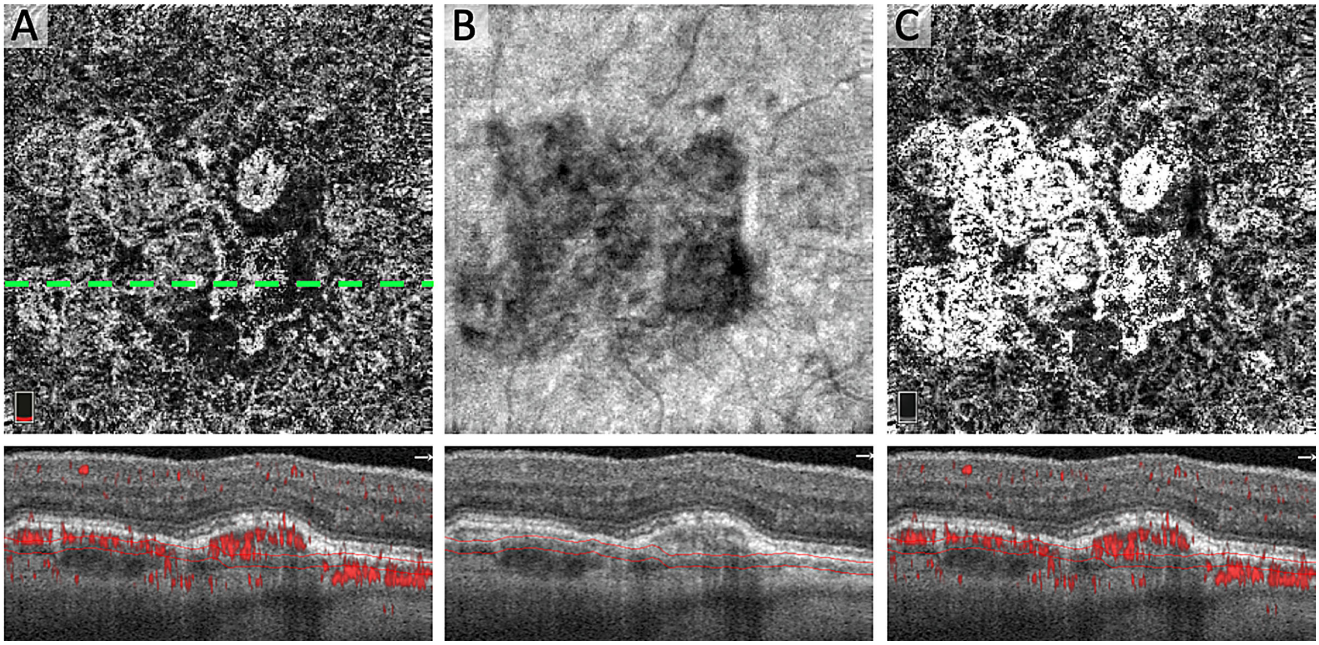

Figure 1. Compensation for OCT Signal and Q-Score in the Choriocapillaris. (**A**) Original en face OCTA of choriocapillaris (Q6) with CNV and OCTA B-scan below from *dotted line* location showing *red flow overlay* and segmentation. (**B**) En face structural OCT of the choriocapillaris with B-scan below showing segmentation and local signal attenuation. (**C**) OCTA after correcting for local OCT and global OCTA signal attenuation.

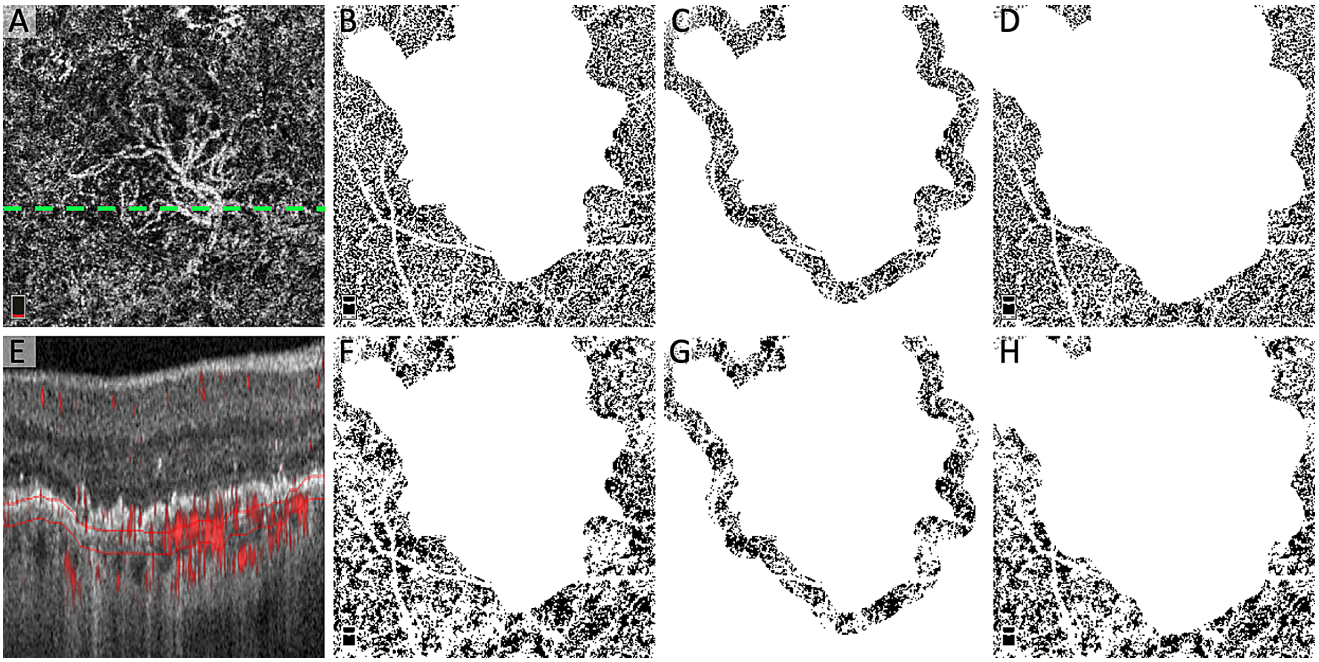

Figure 2. Location of quantitative FD analysis with two binarization thresholding techniques. (**A**) Original OCTA of the choriocapillaris showing CNV and dotted line showing location of B-scan in (**E**). (**B** and **F**) Location of "outside the area of CNV" for quantification of FD after binarization using the local Phansalkar (**B**) and global MinError(I) (**F**) thresholding techniques. (**C** and **G**) Location of the "annulus" for quantification of FD after binarization with Phansalkar (**C**) and MinError(I) (**G**). (**D** and **H**) Location of "outside the annulus" for the quantification of the FD after binarization with Phansalkar (**D**) and MinError(I) (**H**). Note that all *white areas* not attributed to choriocapillaris (including the retinal blood vessel mask) were excluded from analysis. (**E**) OCTA B-scan with *red flow overlay* and choriocapillaris segmentation.

between the two circles are referred to as the "annulus." We measured the FD parameters outside the CNV area, including both the annulus and the area around the annulus, and refer to this region as "outside CNV." We also measured FD parameters in just the area outside of the annulus, but not including it, and refer to this region as "outside annulus" (Fig. 2). On the binarized image of both the annulus and outside areas, we used the Analyze Particles func-

Investigative Ophthalmology & Visual Science

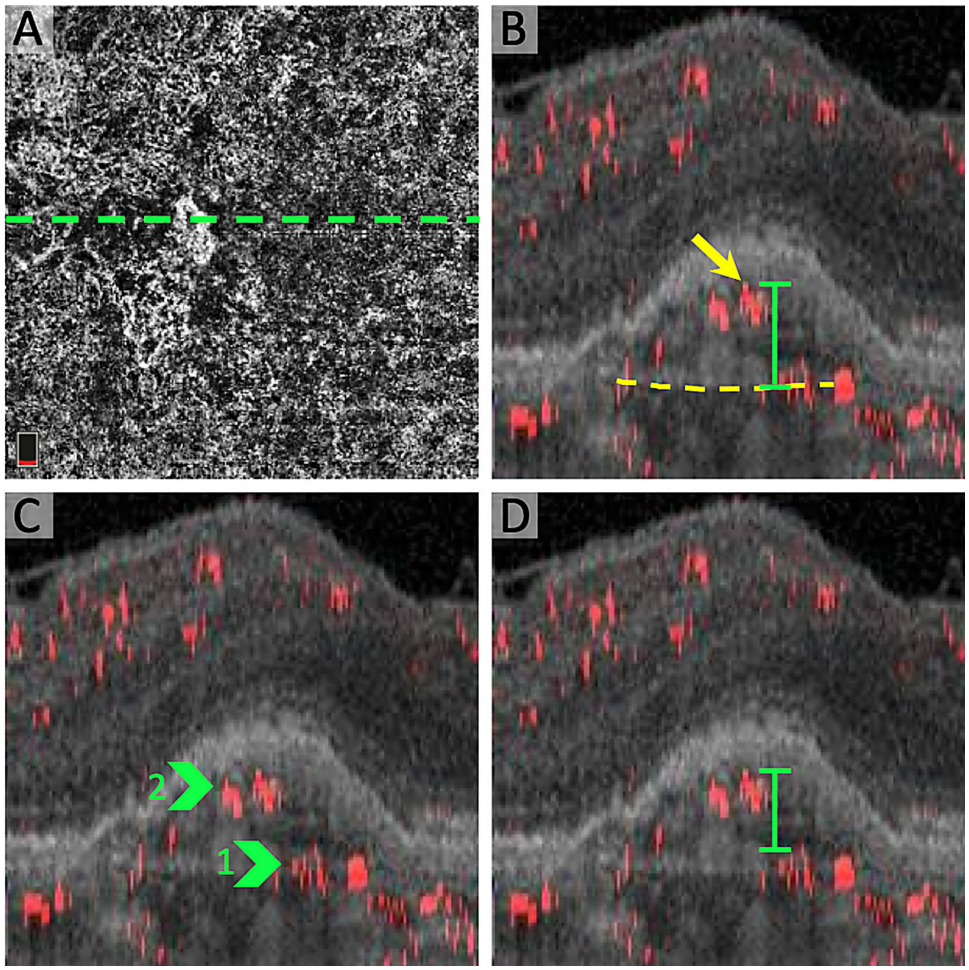

Figure 3. CNV complexity parameters in projection-resolved OCTA. (**A**) En face OCTA of the choriocapillaris with CNV and location of B-scan *(dotted line)*. (**B**) Cross-sectional projection-resolved OCTA showing the "highest CNV flow signal," defined as the distance between Bruch's membrane (*dotted yellow line*) and the most anterior CNV decorrelation signal (*yellow arrow*). (**C**) Cross-sectional projection-resolved OCTA highlighting two "CNV flow layers" (*green arrows*). (**D**) Cross-sectional projection-resolved OCTA with "CNV flow signal thickness," defined as the distance between the two most anterior CNV flow layers (*green*).

tion to quantify the total number of FD (FD count), FD density (FDD), and mean FD size (MFDS) after excluding FD under 24 microns in diameter, which is the estimated size of 1 intercapillary space in healthy eyes under the fovea in OCTA.[25]

CNV Complexity Image Analysis

We implemented a version of projection-resolved OCTA in a custom MATLAB (Mathworks 2015, Natick, MA) program based on the algorithm previously described by Zhang et al.[38] Cross-sectional projection-resolved OCTA was used to quantify 3D CNV complexity. The "highest CNV flow signal" was defined as the greatest distance between Bruch's membrane and the highest point of decorrelation from CNV (Fig. 3).[21] To standardize the approach, a senior grader (PLN) identified and exported the two B-scans with the highest apparent CNV flow signal from the entire imaging volume. The greater of the two measurements was recorded for each eye. The "number of CNV flow layers" was defined as the number of layers of pathologic decorrelation signal that were separated by at least 30 µm in the axial direction. This measurement was performed from the top edge of the deeper flow layer to the bottom edge of the more superficial flow layer. The CNV flow layers that were separated by less than 30 µm were counted as a single CNV flow layer because of limitations in the axial resolution of the device. To ensure that CNV flow layers were not projection artifact, we evaluated the intensity of the decorrelation signal using the Plot Profile tool in FIJI. In CNV membranes with more than one flow layer, we also measured the "CNV flow signal thickness," defined as the distance between the two most anterior CNV flow layers (layers farthest from Bruch's membrane). For eyes with a single CNV flow layer, this value was recorded as zero. Highest CNV flow signal, number of CNV flow layers, and CNV flow signal thickness were recorded for each eye and compared with respect to FD count, FDD, and MFDS using statistical methods.

Statistics

We performed statistical analyses with SPSS version 21 (IBM SPSS Statistics; IBM Corporation, Chicago, IL). Shapiro-Wilk tests were significant, indicating data from CNV complexity

Investigative Ophthalmology & Visual Science

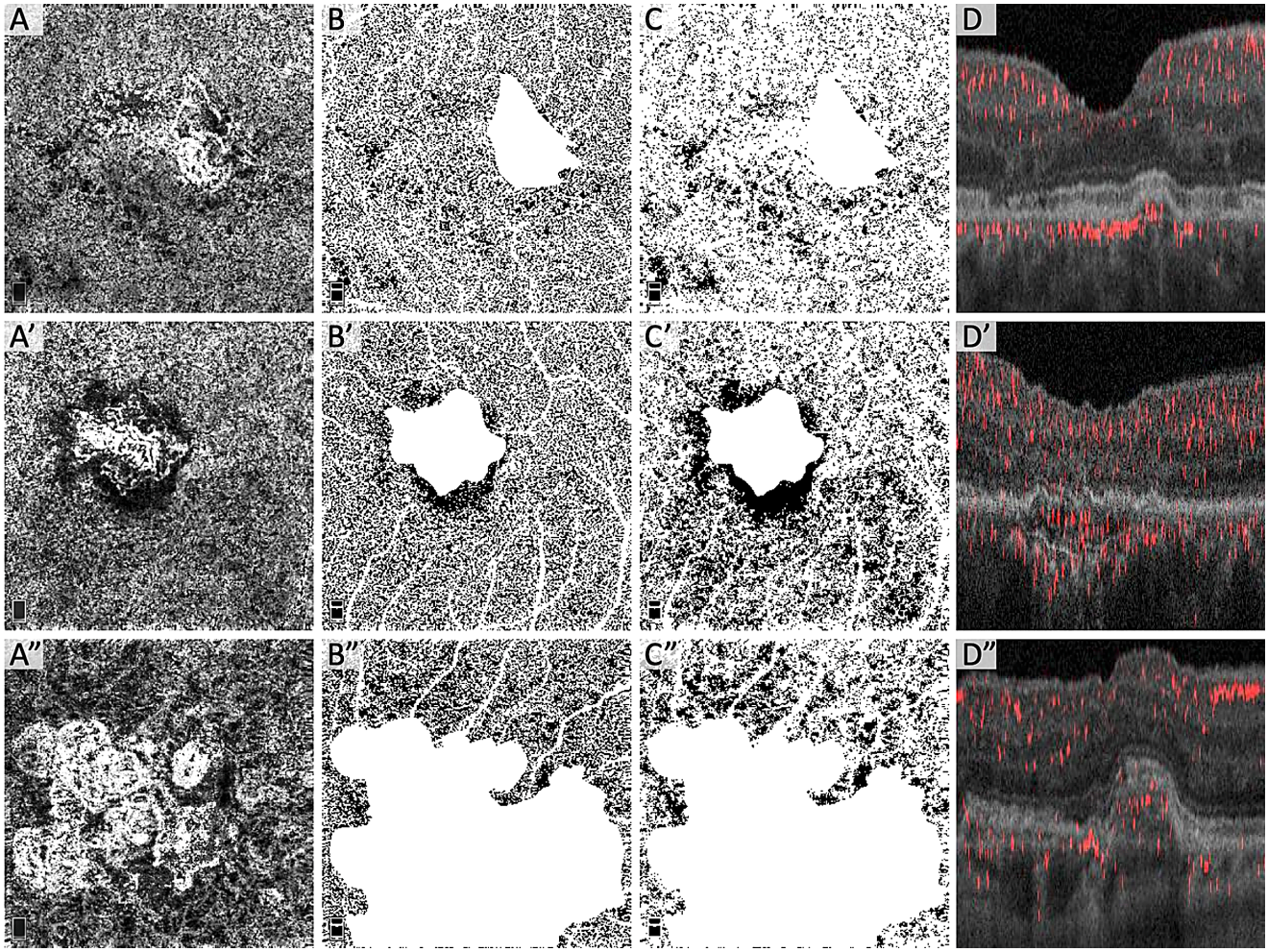

Figure 4. Choriocapillaris FD stratified by number of CNV flow layers. Each row shows images from the same eye with either one (**A–D**), two (**A'–D'**), or three (**A"–D"**) CNV flow layers. (*Column A*) Compensated and normalized en face OCTA of the choriocapillaris. (*Column B*) Local Phansalkar binarized choriocapillaris OCTA of area outside the CNV. (**B'**) Underestimation of the FD in dark halo region using Phansalkar. (*Column C*) Global MinError(I) binarized choriocapillaris OCTA of area outside the CNV. (*Column D*) Cross-sectional projection-resolved OCTA of CNV showing number of CNV flow layers and CNV architecture.

parameters as well as FD count and MFDS deviated from a normal distribution. Levene's tests for equality of variances were not significant, indicating homoscedasticity. Therefore, we performed nonparametric Spearman rank correlations to explore the relationships between linear CNV complexity parameters (CNV flow signal thickness and highest CNV flow signal) and choriocapillaris FD parameters. Spearman rank correlations were also used to assess correlations of CNV complexity and FD compared with age and number of previous injections. The number of CNV flow layers is a categorical variable (values = 1–4). Therefore, we used Kruskal-Wallis H test (one-way ANOVA on ranks) with the post hoc Dunn test to compare FD parameters based on the number of CNV flow layers. We also used the Kruskal-Wallis H test to assess any differences in CNV complexity or FD based on sex, CNV type (PED, subretinal, polypoidal), and unilateral versus bilateral CNV. A P value of less than 0.05 was considered statistically significant.

Results

A total of 29 eyes from 29 patients (age 72.0 ± 13.3 years, 22 females) with CNV were included in this study. Six eyes were treatment naïve and 23 eyes had been previously treated with a median of 8 and a mean of 19.4 ± 23.9 anti-VEGF injections. Eighteen eyes had type 1 (PED) CNV, 4 eyes had type 2 (subretinal) CNV, and 7 eyes had type 4 (PCV) CNV. There were no significant differences in CNV complexity or FD parameters based on CNV type (type 1, 2, or 4) or patient sex (all $P > 0.05$). Age, Q-score, and total number of previous anti-VEGF injections were not significantly correlated with CNV complexity or FD measures (all $P > 0.05$). Although CNV laterality showed no significant relationships to CNV complexity parameters, eyes from patients with bilateral CNV had a lower FD count, higher FDD, and higher MFDS outside the CNV as well as higher FDD and MFDS outside the annulus compared with unilateral CNV with Phansalkar ($P < 0.05$ for all), but these were not significant with MinError(I) ($P > 0.05$ for all). Regarding the number of CNV flow layers, 8 eyes had a single layer, 11 eyes had two layers, and 9 eyes had 3 layers (Fig. 4). One eye with four CNV flow layers was volume-rendered and is included as Supplementary Figure S1.

The correlations between CNV complexity and choriocapillaris FD are reported in Table. The highest CNV flow signal was significantly correlated with lower FD count

Investigative Ophthalmology & Visual Science

Table. Relationship Between CNV Complexity and Choriocapillaris FDs

Location	FD Parameter	Threshold Technique	Average (SD)	Highest Flow		Flow Thickness		No. of Flow Layers	Flow Layers 1–2		Flow Layers 2–3		Flow Layers 1–3	
				r	*P* Value	*r*	*P* Value	*P* Value	*z*	*P* Value	*z*	*P* Value	*z*	*P* Value
Outside Annulus	FD Count	Phansalkar	325 (247)	−0.619*	<0.001	−0.398*	0.032	0.019*	−9.568*	0.016	−2.960	0.439	−12.528*	0.002
	FD Count	MinError(I)	237 (180)	−0.643*	<0.001	−0.394*	0.035	0.010*	−11.000*	0.005	−2.000	0.601	−13.000*	0.002
	FDD	Phansalkar	0.41 (0.05)	0.433*	0.019	0.347	0.065	0.105	–	–	–	–	–	–
	FDD	MinError(I)	0.40 (0.17)	0.413*	0.026	0.443*	0.016	0.076	–	–	–	–	–	–
	MFDS	Phansalkar	92 (24)	0.462*	0.012	0.348	0.064	0.078	–	–	–	–	–	–
	MFDS	MinError(I)	134 (128)	0.451*	0.014	0.462*	0.012	0.043*	10.852*	0.006	−1.838	0.631	9.014*	0.029
Outside CNV	FD Count	Phansalkar	413 (242)	−0.596*	0.001	−0.417*	0.025	0.023*	−9.352*	0.018	−2.939	0.442	−12.292*	0.003
	FD Count	MinError(I)	306 (179)	−0.607*	<0.001	−0.403*	0.030	0.007*	−11.830*	0.003	−1.101	0.774	−12.931*	0.002
	FDD	Phansalkar	0.42 (0.05)	0.436*	0.018	0.369*	0.049	0.076	–	–	–	–	–	–
	FDD	MinError(I)	0.41 (0.16)	0.456*	0.013	0.503*	0.005	0.028*	11.739*	0.003	−3.364	0.379	8.375*	0.043
	MFDS	Phansalkar	89 (21)	0.406*	0.029	0.312	0.100	0.135	–	–	–	–	–	–
	MFDS	MinError(I)	111 (59)	0.422*	0.023	0.473*	0.009	0.028*	11.739*	0.003	−3.364	0.379	8.375*	0.043
Annulus	FD Count	Phansalkar	88 (32)	0.276	0.147	0.016	0.936	0.361	–	–	–	–	–	–
	FD Count	MinError(I)	69 (32)	0.089	0.646	−0.014	0.943	0.819	–	–	–	–	–	–
	FDD	Phansalkar	0.45 (0.06)	0.214	0.265	0.381*	0.042	0.045*	10.784*	0.006	−6.242	0.103	4.542	0.272
	FDD	MinError(I)	0.44 (0.16)	0.397*	0.033	0.507*	0.005	0.011*	12.750*	0.001	−5.000	0.191	7.750	0.061
	MFDS	Phansalkar	86 (18)	0.183	0.342	0.335	0.076	0.034*	11.023*	0.005	−7.162	0.061	3.861	0.351
	MFDS	MinError(I)	105 (54)	0.360	0.055	0.471*	0.010	0.012*	12.750*	0.001	−4.889	0.201	7.861	0.057

Correlation between FD parameters and highest CNV flow or CNV flow thickness were performed with Spearman rank correlations reported with *r* and *P* values. Correlation between FD parameters and the categorical value of number of flow layers were performed with the Kruskal–Wallis H test (one-way ANOVA on ranks) with *P* value reported. If the Kruskal–Wallis was significant, post hoc Dunn tests were reported for individual comparisons between layers with pairwise *z* test statistics and *P* values. The MFDS is reported as diameter in microns.

* $P < 0.05$.

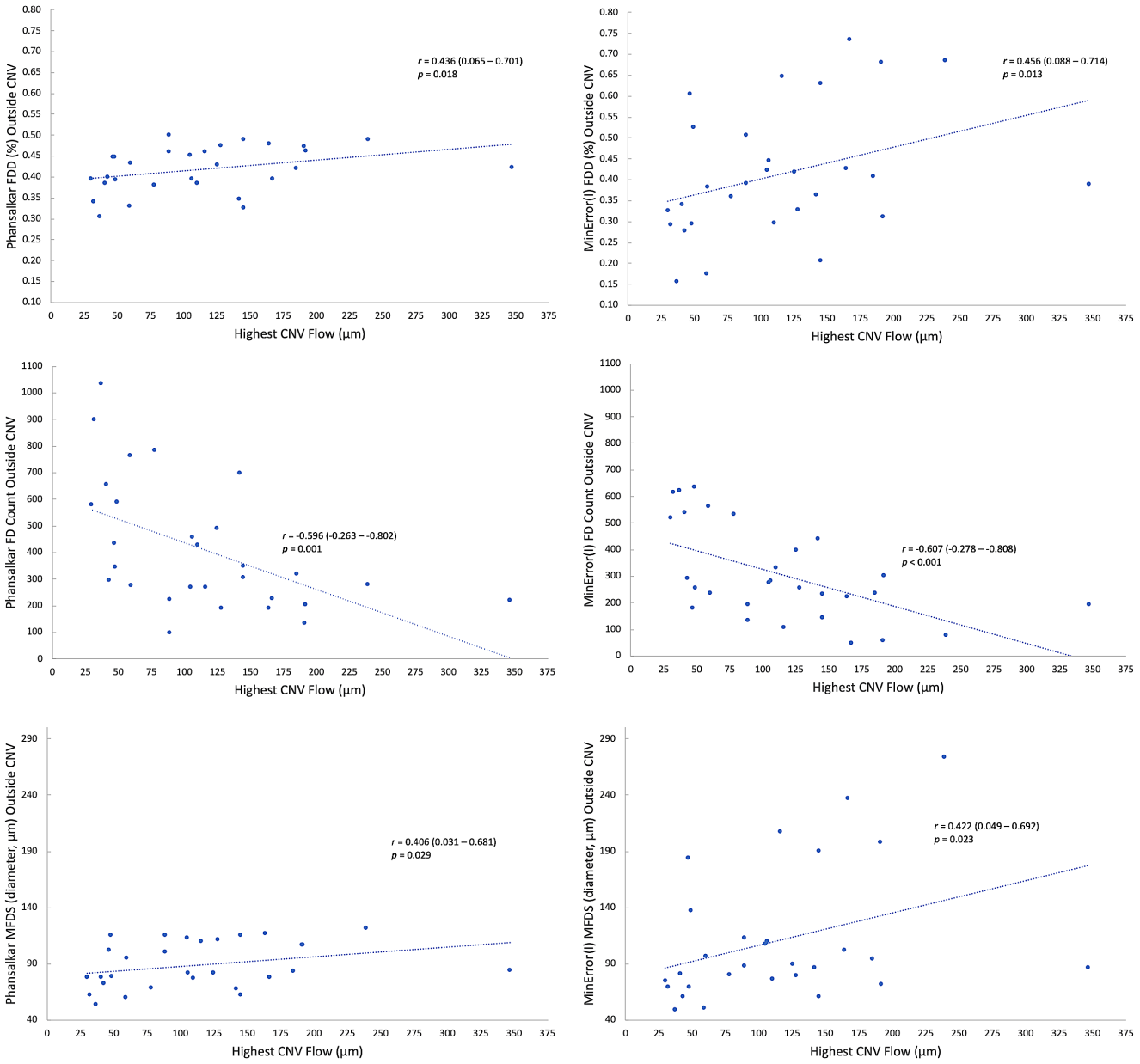

Figure 5. Highest CNV flow signal correlates with choriocapillaris FD outside the CNV in neovascular AMD. (*Top row*) Positive Spearman r correlations between highest CNV flow signal and FDD with Phansalkar (*top left*) and MinError(I) (*top right*). (*Middle Row*) Negative Spearman r correlation between highest CNV flow signal and FD count with Phansalkar (*middle left*) and MinError(I) (*middle right*). (*Bottom row*) Positive Spearman r correlation between highest CNV flow signal and MFDS with Phansalkar (*bottom left*) and MinError(I) (*bottom right*). The *r* values are reported with 95% confidence intervals.

(Phansalkar, $r = -0.596$, $P = 0.001$; MinError(I), $r = -0.607$, $P < 0.001$), higher FDD (Phansalkar, $r = 0.436$, $P = 0.018$; MinError(I), $r = 0.456$, $P = 0.013$), and higher MFDS (Phansalkar, $r = 0.406$, $P = 0.029$; MinError(I), $r = 0.422$, $P = 0.023$) in the area outside the CNV using both thresholding techniques (Fig. 5). Similar significant results were found between highest CNV flow signal and FD parameters in the area outside the annulus (Table). No significant correlations were found between highest CNV flow signal and FD parameters in the annulus, except for FDD with MinError(I) ($r = 0.397$; $P = 0.033$), but this difference was not significant with Phansalkar ($r = 0.214$; $P = 0.265$) (Table). Treatment-naïve eyes showed similar trends in the area outside the CNV and outside the annulus compared with the entire cohort, but these correlations did not reach statistical significance (Supplementary Table S1). Compared with the entire cohort, the direction of the correlations was similar when excluding PCV from the analysis, although fewer parameters were statistically significant (Supplementary Table S2).

CNV flow layer thickness was negatively correlated with FD count in the area outside the annulus and the entire area outside the CNV using both thresholding methods ($P < 0.05$ for all), but not in the annulus ($P > 0.05$ for both). Flow thickness positively correlated with FDD in the area outside the CNV as well as in the annulus with both thresholding methods ($P < 0.05$ for all), but not with Phansalkar in

Investigative Ophthalmology & Visual Science

the area outside the annulus ($P = 0.065$; Table). Flow thickness was positively correlated with MFDS with MinError(I) ($P < 0.05$ for all regions of the choriocapillaris), but not with Phansalkar ($P > 0.05$ for all regions).

Eyes with one CNV flow layer had a significantly higher FD count outside the annulus compared with eyes with two CNV flow layers (Phansalkar; $P = 0.016$; MinError(I); $P = 0.005$) and three CNV flow layers (Phansalkar; $P = 0.002$; MinError(I); $P = 0.002$), with no significant difference between eyes with two versus three CNV flow layers. Similar significant results were found in the entire area outside the CNV, but not in the annulus (Table). Eyes with two compared with one CNV flow layer had greater FDD ($P = 0.003$) and MFDS ($P = 0.003$) in the area outside the CNV with MinError(I), but the overall tests were not significant using Phansalkar ($P = 0.076$ and $P = 0.135$, respectively; Table). In the annulus, eyes with two compared with one CNV flow layer had greater FDD (Phansalkar; $P = 0.006$; MinError(I); $P = 0.001$) and MFDS (Phansalkar; $P = 0.005$; MinError(I); $P = 0.001$).

Discussion

In this study, we found that 3D CNV complexity on projection-resolved OCTA was significantly correlated with a greater density of choriocapillaris FD around the CNV in eyes with neovascular AMD. With the exception of outlining the CNV area, which was performed manually, choriocapillaris FD were calculated using an automated process with a FIJI macro. This streamlined approach included correcting scans for local OCT signal attenuation as well as Q-score variability and used both the local Phansalkar and global MinError(I) binarization threshold techniques to improve its generalizability. The highest CNV flow signal above Bruch's membrane on cross-sections was most consistently correlated with FD parameters in both thresholding methods and was associated with a lower total number of FD as well as a greater density and size of FD. This study provides support for the relationship between choriocapillaris vascular compromise and greater neovascular complexity in CNV membranes. Similar trends were seen when treatment-naïve eyes were analyzed separately (Supplementary Table S2), but these findings were not significant, perhaps owing to the limited sample size ($n = 6$) and type II error. Alternatively, complex CNV growth may occur over time, because CNV in AMD is more likely to present initially as a monolayer.[39]

The thresholding step in image processing of the choriocapillaris is known to affect the quantitative parameters used in our study.[23] Therefore, we used two different forms of binarization to provide assurance that the trends found were due to robust changes in the choriocapillaris that are not influenced by thresholding methods. MinError(I) global thresholding provided consistently accurate representations of FD, rivalling the commonly used Phansalkar method. The smaller sampling window used in local thresholding, such as in the frequently used Phansalkar method, may underestimate the FD when they are larger and coalescent (Fig. 4, B'). Yet, the Phansalkar method has been shown to be more reproducible in the choriocapillaris than other binarization methods.[40,41] Differences in the magnitude of the FD results produced by each method can be appreciated in Figure 5. We were reassured that our findings were consistent, because both methods showed a lower FD count with increases in any of the three CNV complexity parameters (highest CNV flow signal, number of CNV flow layers, and CNV flow layer thickness) in the area outside of CNV and outside the annulus. We also found that increasing CNV flow signal height was correlated with greater FDD and greater FD size (MFDS) using both thresholding methods in these regions. Together, these findings suggest that an increased CNV flow signal height is associated with larger FD that then coalesce, resulting in a lower total number but greater density of FD.

The progression to neovascular AMD is associated with upregulation of VEGF, originating from RPE cells.[4–6,42,43] It is thought that hypoxic RPE cells secrete VEGF causing aberrant angiogenesis, which could potentially nourish and oxygenate the outer retina. Physiologically, the major source of oxygen and nutrients for the RPE and the outer retinal layers is diffusion from the choriocapillaris. Histologic specimens have revealed an obliteration or impairment of the choriocapillaris during the progression of AMD.[5,14,44] In a recent study of AMD, histopathologic specimens of an eye with nonexudative CNV revealed larger gaps between the native choriocapillaris vessels compared with healthy and early AMD.[45] Interestingly, the CNV network in this specimen was reported to have capillary-like vasculature with fenestrations resembling the native choriocapillaris, supporting the hypothesis that these membranes have the capacity to recapitulate the failing choriocapillaris.[45] Although PCV is a distinct entity and should be differentiated from other types of CNV, we found a similar direction in the correlations between CNV complexity and FD parameters when we assessed only type 1 and type 2 CNV (Supplementary Table S2). Fewer parameters were significantly correlated when we excluded eyes with PCV ($n = 7$). We did not find any differences in CNV complexity or FD parameters between any of the CNV types, but further studies with a larger number of eyes with PCV are warranted because the current sample size may not have had the power to detect these differences.

Referred to as the double-layer sign in OCT,[46] neovascular membranes adherent to the inner surface of the RPE are associated with nonexudative CNV and may be the result of striking a balance between choriocapillaris dropout and neovascular compensation. In an OCT study of chronic fibrovascular PED, Rahimy et al.[47] reported multilayered PEDs with neovascular tissue on the undersurface of the RPE separated from the choroid by layers of hyperreflective and presumably fibrous material. These eyes, which maintained good visual acuity, were receiving serial anti-VEGF injections, suggesting that this balance could only be met by the suppression of VEGF. Some eyes even showed an increase in density and numbers of fibrous layers despite continued treatment.[47] Using OCTA, this group also described an evolution from serous PEDs to either persistent serous PED or fibrovascular PED, both of which had very slowly progressing CNV flow area.[39] Some eyes in our study showed a similar fibrovascular phenotype, but with less fibrous material and more vascular layers (Figs. 1 and 3). Eyes in our study may represent an earlier stage of the process described by Rahimy et al.[47] before fibrosis dominates, and where new layers of the CNV grow and are remodeled in the setting hypoxia in an attempt to recapitulate the choriocapillaris.

In a previous study, we found that more complex CNV membranes required more frequent anti-VEGF injections.[21] We suggested that VEGF upregulation may be involved with the thickness and complexity of CNV and the continual remodeling of neovascular architecture.[21] Evidence from our current study shows that these more complex CNV membranes are also linked to choriocapillaris FD in the surrounding choroid. Neovascularization is thought to be the

Investigative Ophthalmology & Visual Science

result of flow impairments in other retinal diseases, including PDR.[19] Knowledge of this pathophysiology led to the implementation of pan-retinal photocoagulation in eyes with PDR, which resulted in significant reduction in vision loss and in retinal neovascularization.[48] Although the location of flow impairment in neovascular AMD is very different from PDR, because AMD is central and choroidal, developing a more complete understanding of the interplay between native and pathologic vasculature in AMD may allow us to identify novel therapeutic approaches.

Previous studies have found an increase in the percentage of FD in the choriocapillaris in the areas immediately surrounding the CNV.[13,49,50] In our study, we did not find consistent correlations between CNV complexity and choriocapillaris FD parameters in the 200-µm annulus around the CNV, with correlations between either flow layer thickness or number of flow layers significant for some but not all FD parameters. These results are most likely due to the effect of the "dark halo," which has been described as an area of absent flow signal in the choriocapillaris surrounding some CNV membranes. Numerous potential explanations have been proposed for this finding, including a vascular steal phenomenon reminiscent of tumors, shadowing artifact, or true ischemia.[50,51] We found that the dark halo was only present in some eyes. For example, the dark halo is seen to partly surround the CNV in Figure 1, is completely absent in Figure 2, and is highly variable in Figure 4. If this halo phenomenon were truly caused by ischemia, we would have expected the annulus FD parameters to be significantly correlated with CNV complexity, which was not the case. From our data, we therefore deduce that the dark halo is more likely an epiphenomenon related to CNV structural or flow artifacts that are cast onto the choroid, rather than true choroidal flow signal impairment. In fact, CNV height was only correlated with FDD in the annulus using the MinError(I) ($P = 0.033$), but not with Phansalkar ($P = 0.265$) (Table). Considering the small window size used for Phansalkar binarization and the tendency of the Phansalkar algorithm to underestimate larger, coalescent FD, it is also possible that areas of dark halo identified as FD by MinError(I) binarization were missed by Phansalkar binarization.

There are several limitations to this study, including the small sample size, which was largely based on our strict exclusion criteria. We excluded any patient from the study who carried a concurrent diagnosis of DM, even in the absence of diabetic retinopathy, because a large number of OCTA studies have shown evidence of early vascular changes, including the choriocapillaris, in patients with DM without retinopathy.[52,53] The small sample size also led to a nonuniform patient cohort regarding treatment status. However, we found no significant correlations with the total number of anti-VEGF treatments, unlike previous studies that reported highly divergent effects of anti-VEGF on the choriocapillaris.[54,55] Further, our treatment-naïve subsample showed similar, although nonsignificant trends compared with the whole cohort (Supplementary Table S1). The current study was also limited by the use of SD-OCTA that, owing to poor penetration of shorter wavelength light, causes signal roll-off when passing through the RPE. This shortcoming is inherent to this device, which we mitigated by compensating for OCT signal attenuation.

In conclusion, we found that 3D CNV vascular complexity was associated with increased FDD in the choriocapillaris around the CNV. We compensated for local and global signal attenuation and quantified FD in two areas of the OCTA image with two different thresholding techniques using a streamlined semiautomated process. This study provides evidence for the importance of choriocapillaris dysfunction in neovascular AMD and shows a potential relationship between choriocapillaris FD and the complexity of CNV membranes. An interesting future study could explore whether choriocapillaris FD or CNV complexity in treatment-naïve eyes is predictive of the frequency of injections in the months and years after diagnosis. It would also be interesting to test whether baseline choriocapillaris FD in treatment-naïve eyes is predictive of future CNV complexity.

Acknowledgments

Supported in part by NIH Grant R01 EY31815 (A.A.F.), and research instrument support by Optovue, Inc., Fremont, California. The funders had no role in study design, data collection and analysis, decision to publish, or preparation of the manuscript.

Disclosure: **P.L. Nesper,** None; **J.X. Ong,** None; **A.A. Fawzi,** None

References

1. Vos T, Allen C, Arora M, et al. Global, regional, and national incidence, prevalence, and years lived with disability for 310 diseases and injuries, 1990–2015: a systematic analysis for the Global Burden of Disease Study 2015. *Lancet.* 2016;388(10053):1545–1602.
2. Mehta S. Age-related macular degeneration. *Prim Care.* 2015;42(3):377–391.
3. Grossniklaus HE, Green WR. Choroidal neovascularization. *Am J Ophthalmol.* 2004;137(3):496–503.
4. Sunness JS, Gonzalez-Baron J, Bressler NM, Hawkins B, Applegate CA. The development of choroidal neovascularization in eyes with the geographic atrophy form of age-related macular degeneration. *Ophthalmology.* 1999;106(5):910–919.
5. McLeod DS, Taomoto M, Otsuji T, Green WR, Sunness JS, Lutty GA. Quantifying changes in RPE and choroidal vasculature in eyes with age-related macular degeneration. *Invest Ophthalmol Vis Sci.* 2002;43(6):1986–1993.
6. Kliffen M, Sharma HS, Mooy CM, Kerkvliet S, de Jong PT. Increased expression of angiogenic growth factors in age-related maculopathy. *Br J Ophthalmol.* 1997;81(2):154–162.
7. Schwesinger C, Yee C, Rohan RM, et al. Intrachoroidal neovascularization in transgenic mice overexpressing vascular endothelial growth factor in the retinal pigment epithelium. *Am J Patbol.* 2001;158(3):1161–1172.
8. Rosenfeld PJ, Brown DM, Heier JS, et al. Ranibizumab for neovascular age-related macular degeneration. *N Engl J Med.* 2006;355(14):1419–1431.
9. Brown DM, Kaiser PK, Michels M, et al. Ranibizumab versus verteporfin for neovascular age-related macular degeneration. *N Engl J Med.* 2006;355(14):1432–1444.
10. McLeod DS, Grebe R, Bhutto I, Merges C, Baba T, Lutty GA. Relationship between RPE and choriocapillaris in age-related macular degeneration. *Invest Ophthalmol Vis Sci.* 2009;50(10):4982–4991.
11. Moult EM, Alibhai AY, Rebhun C, et al. Spatial distribution of choriocapillaris impairment in eyes with choroidal neovascularization secondary to age-related macular degeneration: a quantitative OCT angiography study. *Retina.* 2020;40(3):428–445.
12. Jia Y, Bailey ST, Wilson DJ, et al. Quantitative optical coherence tomography angiography of choroidal

neovascularization in age-related macular degeneration. *Ophthalmology.* 2014;121(7):1435–1444.
13. Treister AD, Nesper PL, Fayed AE, Gill MK, Mirza RG, Fawzi AA. Prevalence of subclinical CNV and choriocapillaris Nonperfusion in fellow eyes of unilateral exudative AMD on OCT angiography. *Transl Vis Sci Technol.* 2018;7(5):19.
14. Seddon JM, McLeod DS, Bhutto IA, et al. Histopathological insights into choroidal vascular loss in clinically documented cases of age-related macular degeneration. *JAMA Ophthalmol.* 2016;134(11):1272–1280.
15. Borrelli E, Uji A, Sarraf D, Sadda SR. Alterations in the choriocapillaris in intermediate age-related macular degeneration. *Invest Ophthalmol Vis Sci.* 2017;58(11):4792–4798.
16. Borrelli E, Shi Y, Uji A, et al. Topographic analysis of the choriocapillaris in intermediate age-related macular degeneration. *Am J Ophthalmol.* 2018;196:34–43.
17. Lutty G, Grunwald J, Majji AB, Uyama M, Yoneya S. Changes in choriocapillaris and retinal pigment epithelium in age-related macular degeneration. *Mol Vis.* 1999;5(35):35.
18. Biesemeier A, Taubitz T, Julien S, Yoeruek E, Schraermeyer U. Choriocapillaris breakdown precedes retinal degeneration in age-related macular degeneration. *Neurobiol Aging.* 2014;35(11):2562–2573.
19. Witmer A, Vrensen G, Van Noorden C, Schlingemann R. Vascular endothelial growth factors and angiogenesis in eye disease. *Prog Retin Eye Res.* 2003;22(1):1–29.
20. Hartnett ME. Pathophysiology and mechanisms of severe retinopathy of prematurity. *Ophthalmology.* 2015;122(1):200–210.
21. Nesper PL, Soetikno BT, Treister AD, Fawzi AA. Volume-rendered projection-resolved OCT angiography: 3D lesion complexity is associated with therapy response in wet age-related macular degeneration. *Invest Ophthalmol Vis Sci.* 2018;59(5):1944–1952.
22. Forsythe JA, Jiang B-H, Iyer NV, et al. Activation of vascular endothelial growth factor gene transcription by hypoxia-inducible factor 1. *Mol Cell Biol.* 1996;16(9):4604–4613.
23. Mehta N, Liu K, Alibhai AY, et al. Impact of binarization thresholding and brightness/contrast adjustment methodology on optical coherence tomography angiography image quantification. *Am J Ophthalmol.* 2019;205:54–65.
24. Chu Z, Zhang Q, Gregori G, Rosenfeld PJ, Wang RK. Guidelines for imaging the choriocapillaris using OCT angiography. *Am J Ophthalmol.* 2020;222:92–101.
25. Chu Z, Cheng Y, Zhang Q, et al. Quantification of choriocapillaris with Phansalkar local thresholding: pitfalls to avoid. *Am J Ophthalmol.* 2020;213:161–176.
26. Koh A, Lee WK, Chen L-J, et al. EVEREST study: efficacy and safety of verteporfin photodynamic therapy in combination with ranibizumab or alone versus ranibizumab monotherapy in patients with symptomatic macular polypoidal choroidal vasculopathy. *Retina.* 2012;32(8):1453–1464.
27. Honda S, Matsumiya W, Negi A. Polypoidal choroidal vasculopathy: clinical features and genetic predisposition. *Ophthalmologica.* 2014;231(2):59–74.
28. Chylack LT, Wolfe JK, Singer DM, et al. The lens opacities classification system III. *Arch Ophthalmol.* 1993;111(6):831–836.
29. Jia Y, Tan O, Tokayer J, et al. Split-spectrum amplitude-decorrelation angiography with optical coherence tomography. *Opt Express.* 2012;20(4):4710–4725.
30. Kraus MF, Liu JJ, Schottenhamml J, et al. Quantitative 3D-OCT motion correction with tilt and illumination correction, robust similarity measure and regularization. *Biomed Opt Express.* 2014;5(8):2591–2613.
31. Schindelin J, Arganda-Carreras I, Frise E, et al. Fiji: an open-source platform for biological-image analysis. *Nat Methods.* 2012;9(7):676–682.
32. Zhang Q, Zheng F, Motulsky EH, et al. A novel strategy for quantifying choriocapillaris flow voids using swept-source OCT angiography. *Invest Ophthalmol Vis Sci.* 2018;59(1):203–211.
33. Zhang Q, Zhang A, Lee CS, et al. Projection artifact removal improves visualization and quantitation of macular neovascularization imaged by optical coherence tomography angiography. *Ophthalmol Retina.* 2017;1(2):124–136.
34. Phansalkar N, More S, Sabale A, Joshi M. Adaptive local thresholding for detection of nuclei in diversity stained cytology images. *2011 International Conference on Communications and Signal Processing*. Kerala, India, IEEE, 2011:218–220.
35. Kittler J, Illingworth J. Minimum error thresholding. *Pattern Recognit.* 1986;19(1):41–47.
36. Cho S, Haralick R, Yi S. Improvement of Kittler and Illingworth's minimum error thresholding. *Pattern Recognit.* 1989;22(5):609–617.
37. Pun T. A new method for grey-level picture thresholding using the entropy of the histogram. *Signal Processing.* 1980;2(3):223–237.
38. Zhang M, Hwang TS, Campbell JP, et al. Projection-resolved optical coherence tomographic angiography. *Biomed Opt Express.* 2016;7(3):816–828.
39. Au A, Hou K, Dávila JP, et al. Volumetric Analysis of vascularized serous pigment epithelial detachment progression in neovascular age-related macular degeneration using optical coherence tomography angiography. *Invest Ophthalmol Vis Sci.* 2019;60(10):3310–3319.
40. Byon I, Alagorie AR, Ji Y, Su L, Sadda SR. Optimizing the repeatability of choriocapillaris flow deficit measurement from optical coherence tomography angiography. *Am J Ophthalmol.* 2020;219:21–32.
41. Chu Z, Gregori G, Rosenfeld PJ, Wang RK. Quantification of choriocapillaris with optical coherence tomography angiography: a comparison study. *Am J Ophthalmol.* 2019;208:111–123.
42. Sarks J, Sarks S, Killingsworth M. Evolution of geographic atrophy of the retinal pigment epithelium. *Eye.* 1988;2(5):552.
43. Zarbin MA. Current concepts in the pathogenesis of age-related macular degeneration. *Arch Ophthalmol.* 2004;122(4):598–614.
44. Nesper PL, Lutty GA, Fawzi AA. Residual choroidal vessels in atrophy can masquerade as choroidal neovascularization on optical coherence tomography angiography: introducing a clinical and software approach. *Retina.* 2018;38(7):1289–1300.
45. Chen L, Messinger JD, Sloan KR, et al. Nonexudative macular neovascularization supporting outer retina in age-related macular degeneration: a clinicopathologic correlation. *Ophthalmology.* 2020;127(7):931–947.
46. Shi Y, Motulsky EH, Goldhardt R, et al. Predictive value of the OCT double-layer sign for identifying subclinical neovascularization in age-related macular degeneration. *Ophthalmol Retina.* 2019;3(3):211–219.
47. Rahimy E, Freund KB, Larsen M, et al. Multilayered pigment epithelial detachment in neovascular age-related macular degeneration. *Retina.* 2014;34(7):1289–1295.
48. Early Treatment Diabetic Retinopathy Study Research Group. Early photocoagulation for diabetic retinopathy: ETDRS report number 9. *Ophthalmology.* 1991;98(5):766–785.
49. Alagorie AR, Verma A, Nassisi M, et al. Quantitative assessment of choriocapillaris flow deficits surrounding choroidal neovascular membranes. *Retina.* 2020;40(11):2106–2112.
50. Scharf JM, Corradetti G, Alagorie AR, et al. Choriocapillaris flow deficits and treatment-naïve macular neovascularize-

tion secondary to age-related macular degeneration. *Invest Ophthalmol Vis Sci.* 2020;61(11):11.

51. Coscas F, Lupidi M, Boulet JF, et al. Optical coherence tomography angiography in exudative age-related macular degeneration: a predictive model for treatment decisions. *Br J Ophthalmol.* 2019;103(9):1342–1346.
52. Cao D, Yang D, Huang Z, et al. Optical coherence tomography angiography discerns preclinical diabetic retinopathy in eyes of patients with type 2 diabetes without clinical diabetic retinopathy. *Acta Diabetol.* 2018;55(5):469–477.
53. Nesper PL, Roberts PK, Onishi AC, et al. Quantifying microvascular abnormalities with increasing severity of diabetic retinopathy using optical coherence tomography angiography. *Invest Ophthalmol Vis Sci.* 2017;58(6):BIO307–BIO315.
54. Rispoli M, Savastano MC, Lumbroso B. Quantitative vascular density changes in choriocapillaris around CNV after anti-VEGF treatment: dark halo. *Ophthalmic Surg Lasers Imaging Retina.* 2018;49(12):918–924.
55. Hikichi T, Agarie M. Reduced vessel density of the choriocapillaris during anti-vascular endothelial growth factor therapy for neovascular age-related macular degeneration. *Invest Ophthalmol Vis Sci.* 2019;60(4):1088–1095.

Supplementary Material

Supplementary Video. Volume-rendering of complex CNV with four flow layers. (A) Original OCTA of the choriocapillaris. (B) Projection-resolved cross-sectional OCTA with red flow overlay. Green arrows point to four individual flow layers. (C) Volume-rendered CNV video starting with flat lower portion closest to the choroid for orientation. (D) MinError(I) binarization of the choriocapillaris. (E) Phansalkar binarization of the choriocapillaris.

Investigative Ophthalmology & Visual Science